## AGE MODEL

The age model for St. Stephens Quarry (SSQ, Fig. DR1) is derived from oxygen isotope- and magneto-stratigraphy, together with planktic foraminiferal, calcareous nannofossil and dinoflagellate biostratigraphy (Fig. DR2 and DR3). Since the publication of Miller et al. (2008) we have resampled the core and studied the archive core at the Alabama Geological Survey, this has resulted in some adjustments to the sample depth. Furthermore, we interpreted assemblages of organic walled dinoflagellate cysts (dinocysts) to re-evaluate the sequence stratigraphic interpretations of the SSQ corehole. The main change relative to the previous interpretations (Miller et al., 2008; Katz et al., 2008) concerns the identification of a hiatus (at 46.25 m) near the base of Chron C13n, just above the sequence boundary dividing the Yazoo and Red Bluff/Bumpnose Formations (46.97 m). The hiatus is extensive enough (~190 kyr) to encompass most of the peak oxygen isotope values used to recognize Oi-1. The age assigned to the hiatus is 33.55 to 33.36 Ma.

## SEQUENCE STRATIGRAPHY

In order construct a chronostratigraphy for the isotope- and temperature data from SSQ we have first revisited the sequence stratigraphic interpretations as postulated by Miller et al. (2008, 2009) using dinocyst assemblage information (Fig. DR2). The premise of dinocysts as indicators of water depth is founded on the observation that different morphological groups dominated in specific environments at proximal to distal settings (see e.g., Brinkhuis, 1994; Jaramillo and Oboh-Ikuenobe, 1999; Pross and Brinkhuis, 2005). Typically, open oceanic assemblages are dominated by taxa such as *Impagidinium* spp., *Nematosphaeropsis* spp. (the latter two being grouped under the *Impagidinium* complex, cpx) and *Spiniferites* spp., with the exception of *Spiniferites pseudofurcatus*. High relative abundances of these taxa are therefore considered indicative of phases of high relative sea level, with maximum abundances indicating maximum flooding surfaces (MFSs). Taxa belonging to the *Glaphyrocysta - Areoligera* cpx are often found associated with inner neritic, high energy environments. Hence, abundant *Glaphyrocysta-Areoligera* cpx appears consistently related to third order transgressive systems tracts in sequence stratigraphic terms, and thus to sea level rise in neritic settings (e.g., Crouch and Brinkhuis, 2005; Sluijs et al., 2008; Sluijs and Brinkhuis, 2009). Finally, representatives of the Goniodomid family (primarily *Homotryblium* spp. at SSQ) are typically found associated with restricted lagoonal-like conditions. We therefore interpreted high loadings of these taxa to be indicative of low relative sea level. Restricted conditions are also indicated by high percentages of terrestrial organic matter (e.g. pollen and spores) (Fig. DR2). Combining this information allows us to recognize sequence boundaries (SBs) and MFSs. In addition, the evaluation of the relative abundance of these palynological indicators enabled us to define sequence stratigraphic specific systems tracts (Fig. DR2).

In general, our palynological data support the observations as summarized in Miller et al. (2008, 2009 and references therein). The sequence boundaries in the middle of the Pachuta Member of the Yazoo Formation (50.4 m [165.3 feet], SB1), at the top of the Shubuta Member of the Yazoo Formation (47 m [154.1 feet], SB3) and at the top of the Red Bluff/Bumpnose Formation (40.5 m [133 feet], SB5) are in accordance with previous studies. However, there are some sensitive modifications to previous sequence stratigraphic interpretations.

An important modification to previous lithostratigraphic based interpretations is the recognition of a sequence boundary in the upper part of the Pachuta Member of the Yazoo Formation (49 m [161 feet], SB2), approximately corresponding to the precursor (EOT-1)

isotope shift. Miller et al. (2008) tentatively interpreted this horizon as a maximum flooding surface, mainly based on a high abundance of the benthic foraminifer *Uvigerina*. However, dinocyst assemblage data (this study) show that this horizon is associated with high loadings of Goniodomid taxa and subsequently increasing abundance of the *Areoligera-Glaphyrocysta* cpx above 49 m [161 feet]. This suggests a change from a shallowing upward highstand systems track (HST) to a deepening upward transgressive systems track (TST) which could indicate a sequence boundary since regressive lowstand deposits are not generally found in the coastal plain (Miller et al., 2005, 2008). A similar interpretation was proposed by Miller et al. (2009) and Katz et al. (2008) based on the observation of increasing glauconitic beds above this level. Glauconite sands typically overlie sequence boundaries in transgressive sequences, since they are formed under highly dynamic circumstances with exposure to sedimentary winnowing (Miller et al., 2005 and references therein). However, no distinct surface was noted and the interpretation of a sequence boundary is largely determined by the facies successions inferred from dinocysts and requires additional testing/verification elsewhere, as detailed sequence stratigraphic studies on the EOT-1 are rare.

Except from a relatively minor decline in open oceanic taxa, no dramatic change in water-depth is detected based on dinocysts assemblages across the sequence boundary identified at the contact between the Yazoo and the Red Bluff/Bumpnose Formations (47 m [154.1] feet, SB3). This suggests that no major hiatus is involved. We therefore follow Miller et al. (2008) in assigning a very small hiatus (33.59 – 33.62 Ma) at this level.

From previous studies it appeared that at SSQ no hiatus was created by the supposedly largest sea-level fall of the Cenozoic at times of the Oi-1 (see e.g. Katz et al., 2008; Miller et al. 2008, 2009). The base of Oi-1 is positioned at the onset of the normal Chron C13n (Zachos et al., 1996). This information precludes that the sequence boundary between the Shubuta Member and the Red Bluff/Bumpnose Formation (SB3) is associated with Oi-1. If a substantial sea-level drop, and therefore a hiatus would be associated with the Oi-1, it should be sought above the reversal between Chrons C13r and C13n. At SSQ, the onset of Chron C13n is between 46.36 and 46.02 m (152.1 and 151 feet [151.75 mid-point]; Miller et al., 1993). Remarkably, dinocyst assemblages at this level are indicative of an increase of relative sea-level, which is in accordance with the tentative maximum flooding surface that was recognized at this level by Miller et al. (2008). We interpret this horizon as reflecting a hiatus; we suggest that deposition re-incepted in conjunction with rapidly increasing relative sea-level just after Oi-1. This is further elaborated by the absence of dinocyst taxa typically encountered around the Oi-1 horizon in the Mediterranean and in the North Atlantic such as *Areosphaeridium diktyoplokum* (Brinkhuis and Biffi, 1993; Brinkhuis, 1994; Eldrett et al., 2004).

Additionally, we have tentatively identified a sequence boundary at 45.4 m (149 ft) (SB4) (Fig. DR2, DR4). The expanded high systems tract of the relatively shallow *Hanzawaia* biofacies is elaborated by the palynological associations; as indicated by increasing abundance of Goniodomids and terrestrial palynomorphs. A clear sequence boundary overlies of the succession at 40.5 m (133 ft) (SB5) at the top of the Red Bluff/Bumpnose Formation (Fig. DR2, DR4).

Using this sequence stratigraphic model, we used the bio- and magnetostratigraphic information provided by Miller et al. (2008) to establish an age-model for SSQ (Fig. DR3, Table DR1). We correlated the benthic foraminiferal $\delta^{18}O$ and $\delta^{13}C$ record of SSQ to that of DSDP Site 522 and ODP Site 744 (Zachos et al., 1996) to as accurately as possible establish durations for the hiatus associated with Oi-1 and the interval above the Oi-1 (Table DR1). The

hiatus corresponding to the Oi-1 provides a plausible explanation for the $\delta^{18}O$ record at SSQ, in which no shift with intermediate $\delta^{18}O$ values was recorded (see e.g., Katz et al., 2008). With our new age model, the hiatus in the lower Oligocene is ~190 kyr. Our results are in line with previous studies (e.g., Pasley and Hazel, 1990; Mancini, 2000), that have estimated a time-gap of between 191,000 to 288,000 years.

## BIO- AND LITHO-STRATIGRAPHY

The placement of the E/O boundary at SSQ has been widely debated. The highest occurrence (HO) of *Hantkenina* is suppressed in the SSQ corehole (see Miller et al., 2008). We estimate the E/O boundary to be at 47.37 m (155.4 ft) based on the highest common occurrence (HCO) of *Pseudohastigerina micra*, which is synchronous with the HO of *Hantkenina* in Tanzania (Wade and Pearson, 2008; Wade et al., 2011). In terms of the lithostratigraphy, this places the E/O boundary in the very uppermost Shubuta Marl of the Yazoo Formation (Fig. DR3, DR4), consistent with previous studies (e.g., Mancini, 1979; Waters and Mancini, 1982). Unlike earlier work based on outcrop sections in the US Gulf Coastal Plain (e.g. Bybell and Poore, 1983; Keller, 1985) we did not find reworking of *Hantkenina*.

## PLANKTIC FORAMINIFERA PRESERVATION

Planktic foraminifera are generally well preserved and glassy beneath the light microscope, with preservation comparable to Tanzania (Pearson et al., 2008). The excellent preservation confirmed in SEM images that show clear pores and wall structures (Fig. 6 in Miller et al., 2008). Preservation deteriorates to moderate in the carbonate rich intervals which were studied for biostratigraphic purposes only. Above 46.24 m the samples are highly lithified, with deterioration in the planktic foraminiferal preservation and many specimens infilled and/or with calcite overgrowth. Therefore we have less confidence in the planktic foraminiferal Mg/Ca results in the interval from 36 to 46.15 m (118 -151.4 ft) (Fig. DR4). Furthermore, planktic foraminiferal assemblages in the upper interval are of low diversity and rare in samples from 45.8 to 46 m (151 to 150.35 ft).

## TRACE ELEMENT GEOCHEMISTRY METHODS AND PLANKTIC FORAMINIFERAL PALEOBIOLOGY

Standard procedures were used for cleaning planktic foraminifera for trace element ratios. We included physical withdrawal of contaminants using the binocular microscope, a clay-removal step, two oxidation steps, a reductive step and one dilute-acid leach. Foraminiferal Mg/Ca ratios were measured using high-resolution inductively-coupled-plasma mass spectrometry at the Institute of Marine and Coastal Sciences at Rutgers University (long-term precision <2% relative standard deviation) following the method outlined in Rosenthal et al., (1999). Mg/Ca ratios are reported in Table DR2.

Ontogenetic stable isotope data indicate that *Turborotalia ampliapertura* were asymbiotic (Wade, unpublished data), however, trace elements within *T. ampliapertura* may have significant offsets through ontogeny (Wade et al., 2009) and thus it is important to use a narrow size fraction. We restricted specimens to the 250 to 300 μm size fraction for Mg/Ca analysis.

The planktic foraminiferal species *Dentoglobigerina pseudovenezuelana* were analyzed for trace elements in two samples (43.0m and 46.7m). We find a 1.5°C offset between the

temperatures recorded by *T. ampliapertura* and *D. pseudovenezuelana* in the sample at 46.7 m (Table DR3; Fig. DR5). This is highly consistent with the offset (0.4‰, equivalent to 1.8°C) recorded in oxygen isotopes in Zone O1 of Tanzania (Wade and Pearson, 2008), and confirms *D. pseudovenezuelana* occupied a deeper dwelling thermocline habitat.

## STABLE ISOTOPE GEOCHEMISTRY METHODS

Foraminifera were reacted in phosphoric acid at 90°C for 15 minutes in an automated peripheral connected to a Micromass Optima mass spectrometer in the Department of Earth and Planetary Sciences at Rutgers University. Analytical precision of replicate analyses of NBS-19 and an internal laboratory standard yield deviations of 0.08‰ for $\delta^{18}O$. Stable isotope values are reported versus V-PDB (Table DR3).

## $TEX_{86}$ PALEOTHERMOMETRY

Organic molecules were extracted from powdered and freeze- dried sediments with dichloromethane (DCM)/ methanol (MeOH) (9:1, v/v) using an accelerated solvent extraction technique (Dionex). Excess solvent was removed using rotary evaporation under vacuum. The total extracts were separated in apolar and polar fractions over an activated $Al_2O_3$ column using hexane:dichloromethane (DCM) (1:1, v/v) and DCM:MeOH (1:1), respectively.

The polar fraction was dissolved in a 99:1 hexane/propanol solvent, and filtered using a 0.45 μm, 4 mm diameter polytetrafluoroethylene (PTFE) filter, before being analyzed using a high performance liquid chromatography/atmospheric pressure positive ion chemical ionization mass spectrometry (HPLC/APCI-MS). HPLC/APCI-MS analyses were conducted according to Schouten et al. (2007) using an Agilent 1100 series LC/MSD SL and separation and a Prevail Cyano column (2.1 x 150 mm, 3 mm; Alltech), maintained at 30 °C. The GDGTs were eluted using a changing mixture of hexane and propanol as follows, 99% hexane: 1% propanol for 5 minutes, then a linear gradient to 1.8% propanol in 45 minutes. Flow rate was 0.2 ml per minute. Single ion monitoring was set to scan the 5 $[M+H]^+$ ions of the GDGTs with a dwell time of 237 ms for each ion. $TEX_{86}$ values were calculated according to Schouten et al. (2002) and Kim et al. (2010). Data are tabulated in Table DR4.

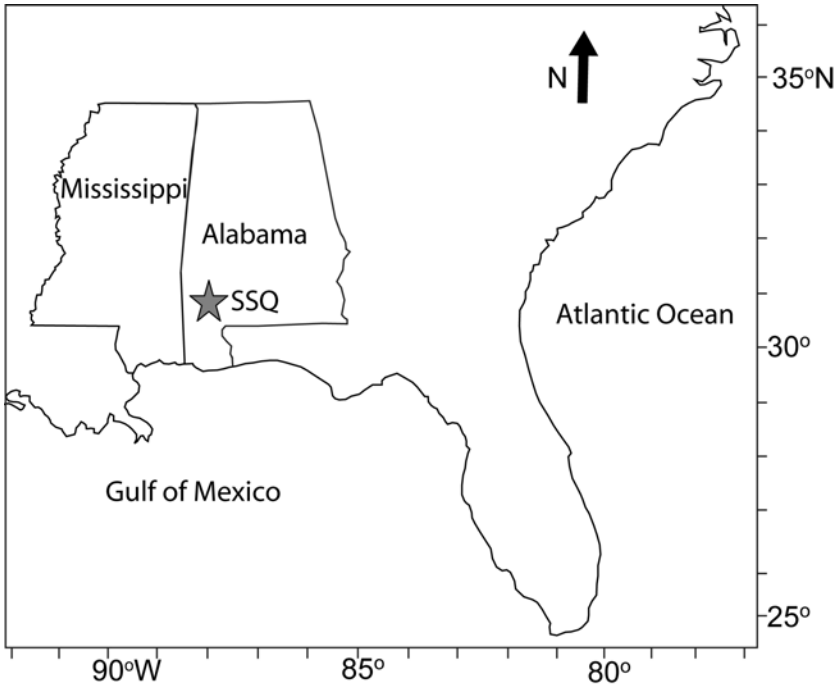


**Figure DR1**. Location of St. Stephens Quarry (SSQ), Alabama.

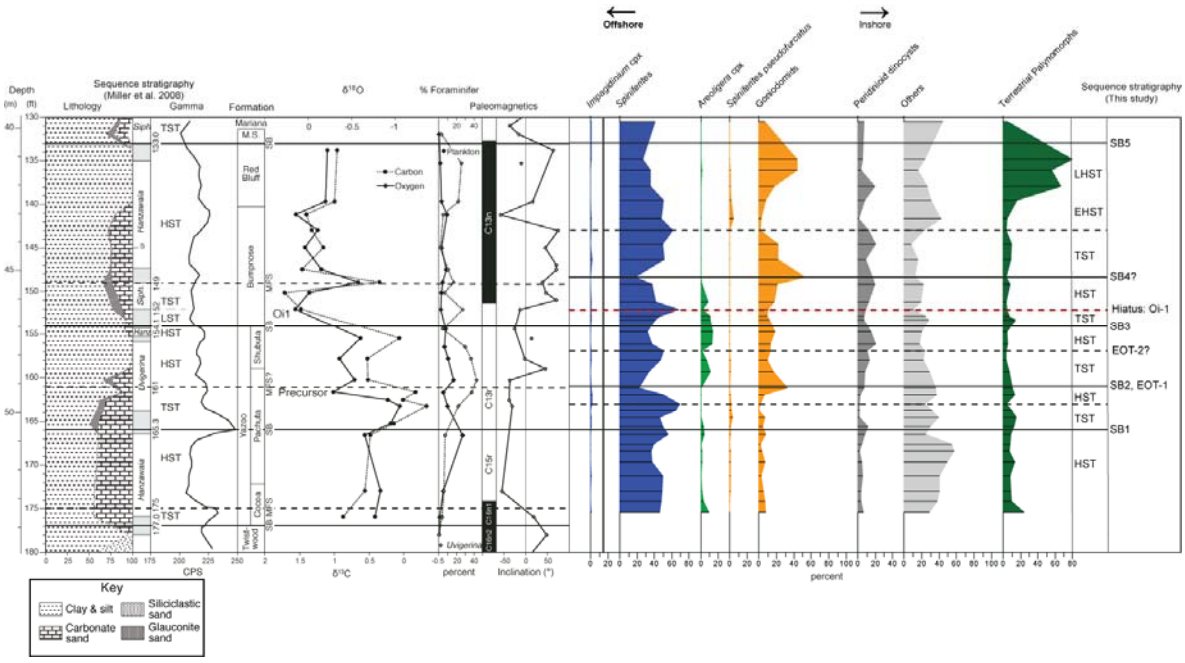


**Figure DR2**. Litho-, magneto- and sequence stratigraphic summary. Lithology, gamma-, and $\delta^{18}O$ data from Miller et al. (1993, 2008). Relative abundance of paleoenvironmentally important palynological groups and sequence stratigraphic interpretation (this study). Continuous lines indicate sequence boundaries, dashed lines indicate maximum flooding surfaces. Note the hiatus just above SB3 and below the early Oligocene maximum flooding surface indicated by the red line.

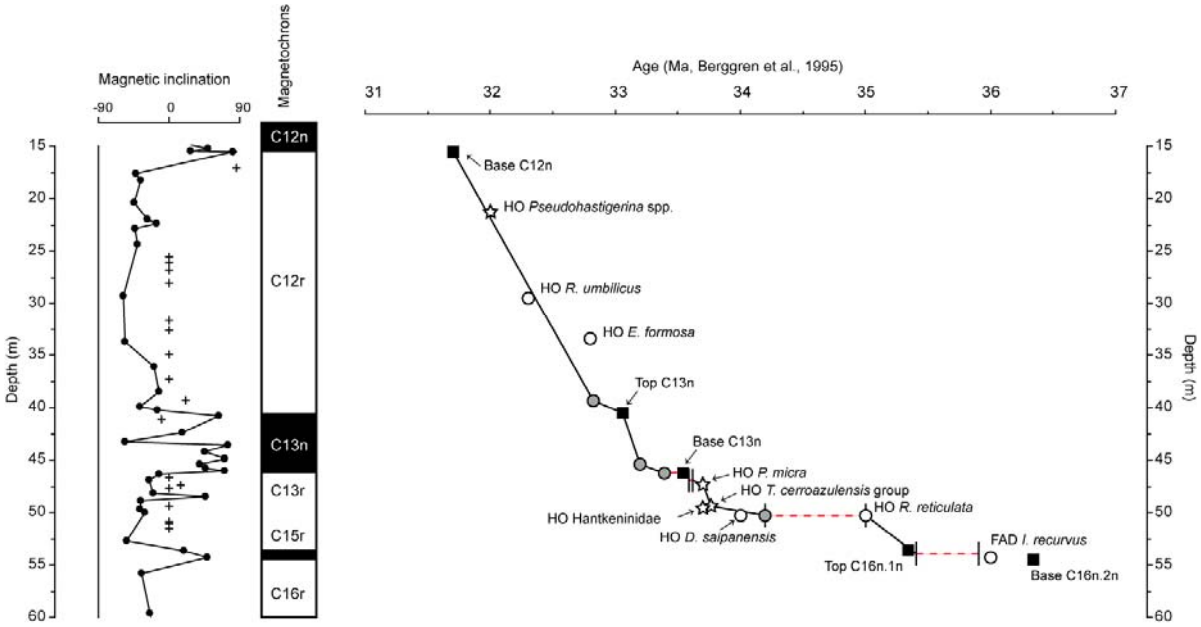


**Figure DR3**. Age-Depth plot with magnetic inclination data and interpretation. Black squares indicate paleomagnetic tie-points, stars = planktic foraminifer events, white circles = calcareous nannofossil events and gray circles = carbon isotopic correlations. Vertical dashed lines indicate the position of hiatuses.

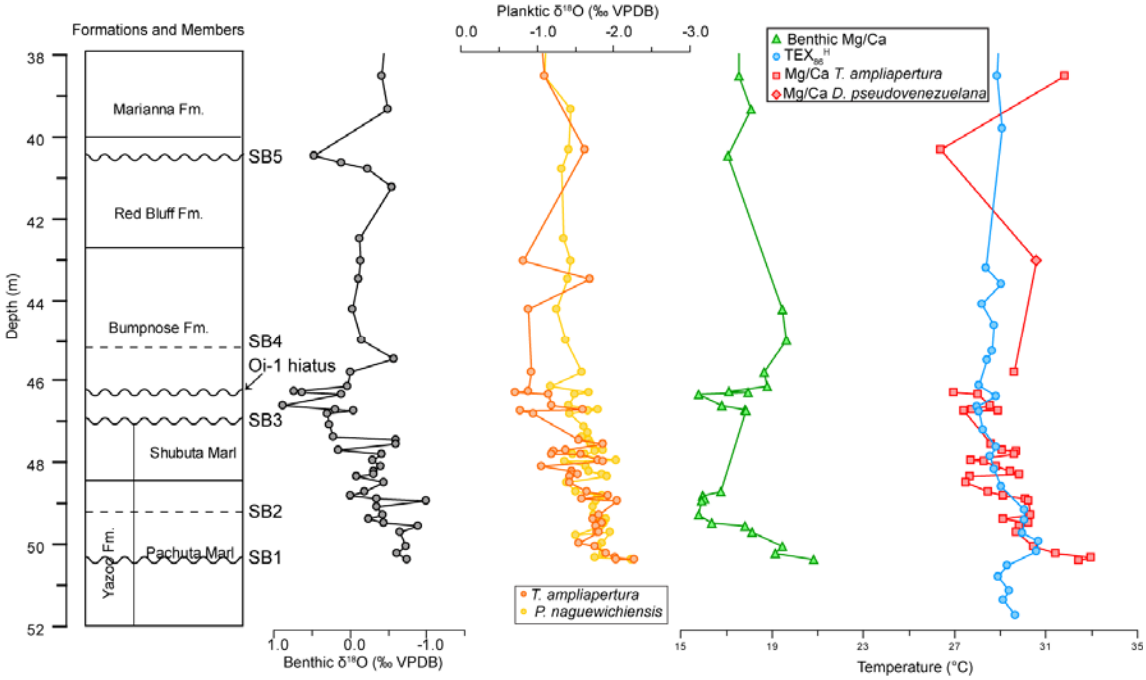


**Figure DR4**. Oxygen isotope and sea surface temperature data against depth. The lithostratigraphy is shown on the left. Wavy lines indicate hiatuses, in most cases associated with sequence boundaries. Continuous horizontal lines indicate the position of formation boundaries (cf. Miller et al., 2008), dashed horizontal lines indicate newly identified (para)sequence boundaries. The E/O boundary is at 47.37 m.

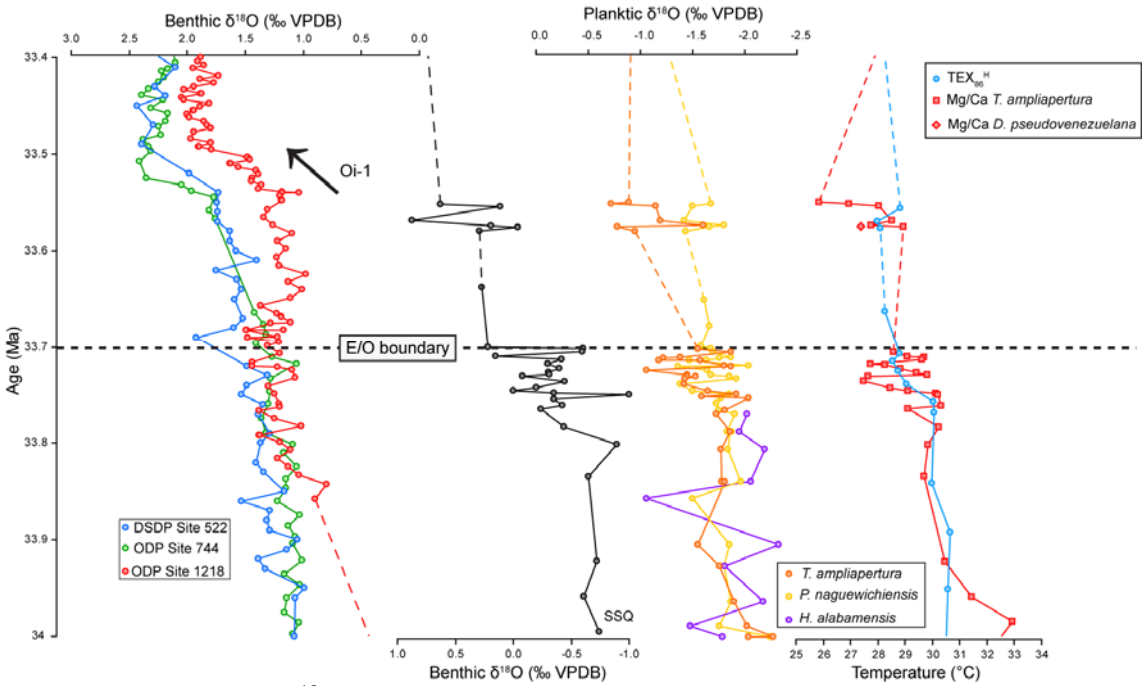


**Figure DR5.** Detail of $\delta^{18}O$ and sea surface temperature (SST) changes through the EOT. Benthic foraminiferal $\delta^{18}O$ record from SSQ (Katz et al., 2008), ODP Site 522, 744 and 1218 (Zachos et al., 1996; Coxall et al., 2005); Planktic foraminiferal $\delta^{18}O$, Mg/Ca and $TEX_{86}$ SSTs from SSQ (this study).

**REFERENCES**

Brinkhuis, H., 1994, Late Eocene to Early Oligocene dinoflagellate cysts from the Priabonian type-area (Northeast Italy): biostratigraphy and paleoenvironmental interpretation: Palaeogeography. Palaeoclimatology, Palaeoecology, v.107, p.121-163.

Brinkhuis, H. and Biffi, U., 1993, Dinoflagellate cyst stratigraphy of the Eocene/Oligocene transition in central Italy: Marine Micropaleontology, v.22, p.131-183.

Bybell, L.M., and Poore, R.Z., 1983, Reworked *Hantkenina* specimens at Little Stave Creek, Alabama: Gulf Coast Association of Geological Societies Transactions, v. 33, p. 253–256.

Coxall, H. K., Wilson, P. A., Pälike, H., Lear, C. H., and Backman, J. 2005, Rapid stepwise onset of Antarctic glaciation and deeper calcite compensation in the Pacific Ocean: Nature, v.433, p. 53-57.

Crouch, E.M. and Brinkhuis, H., 2005, Environmental change across the Paleocene–Eocene transition from eastern New Zealand: A marine palynological approach: Marine Micropaleontology, v. 56, p.138-160.

Eldrett, J.S., Harding, I.C., Firth, J.V. and Roberts, A.P., 2004, Magnetostratigraphic calibration of Eocene-Oligocene dinofagellate cyst biostratigraphy from the Norwegian-Greenland Sea: Marine Geology, v. 204, p.91-127.

Jaramillo, C.A. and Oboh-Ikuenobe, F.E., 1999, Sequence stratigraphic interpretations from palynofacies, dinocyst and lithological data of Upper Eocene-Lower Oligocene strata in southern Mississippi and Alabama, U.S. Gulf Coast: Palaeogeography, Palaeoclimatology, Palaeoecology, v. 145, p.259-302.

Katz, M.E., Miller, K.G., Wright, J.D., Wade, B.S., Browning, J.V., Cramer, B.S. and Rosenthal, Y., 2008, Stepwise transition from the Eocene greenhouse to the Oligocene icehouse: Nature Geoscience, v. 1, p.329-334.

Keller, G., 1985, Eocene and Oligocene stratigraphy and erosional unconformities in the Gulf of Mexico and Gulf Coast: Journal of Paleontology, v. 39, p. 882–903.

Kim, J.-H., van der Meer, J., Schouten, S., Helmke, P., Willmott, V., Sangiorgi, F., Koç, N., Hopmans, E.C. and Sinninghe Damsté, J.S, 2010. New indices and calibrations derived from the distribution of crenarchaeal isoprenoid tetraether lipids: Implications for past sea surface temperature reconstructions. Geochimica et Cosmochimica Acta, v. 74, p. 4639-4654.

Mancici, E.A. 1979, Eocene-Oligocene Boundary in southwest Alabama: Transactions – Gulf Coast Association of Geological Societies, v. XXIX, p. 282-289.

Mancini, E.A. 2000, Sequence stratigraphy and chronostratigraphy of upper Eocene and lower Oligocene strata, Eastern Gulf Coastal Plain: Gulf Coast Association of Geological Societies Transactions, v. L, p.379 – 388.

Miller, K.G., Thompson, P.R., and Kent, D.V., 1993, Integrated stratigraphy of the Alabama coastal plain: Relationship of upper Eocene to Oligocene unconformities to glacioeustatic change: Paleoceanography, v. 8, p. 313–331.

Miller, K.G., Kominz, M.A., Browning, J.V., Wright, J.D., Mountain, G.S., Katz, M.E., Sugarman, P.J., Cramer, B.S., Christie-Blick, N. and Pekar, S.F., 2005, The Phanerozoic Record of Global Sea-Level Change: Science, v. 310, p. 1293-1298.

Miller, K.G., Browning, J.V., Aubry, M.P., Wade, B.S., Katz, M.E., Kulpecz, A.A. and Wright, J.D., 2008, Eocene–Oligocene global climate and sea-level changes: St. Stephens Quarry, Alabama: Geological Society of America Bulletin, v. 120, p. 34-53.

Miller, K.G., Wright, J.D., Katz, M.E., Wade, B.S., Browning, J.V., Cramer, B.S. and Rosenthal, Y., 2009, Climate threshold at the Eocene-Oligocene transition: Antarctic ice sheet influence on ocean circulation: Geological Society of America Special Papers, v. 452, p. 169-178.

Pasley, M.A., Hazel, J.E., 1990, Use of organic petrology in graphic correlation of biostratigraphic data in sequence stratigraphic interpretations: example from the Eocene–Oligocene boundary section, St. Stephens Quarry, Alabama: Trans. Gulf Coast Assoc. Geol. Soc. v. 40, p. 661–683.

Pearson, P.N., McMillan, I.K., Wade, B.S., Dunkley Jones, T., Coxall, H.K., Bown, P.R. and Lear, C.H., 2008. Extinction and environmental change across the Eocene-Oligocene boundary in Tanzania. Geology, v. 36, p. 179–182.

Pross, J. and Brinkhuis, H., 2005, Organic-walled dinoflagellate cysts as paleoenvironmental indicators in the Paleogene; a synopsis of concepts: Palaeontologische Zeitschrift, v. 79, p. 53-59.

Rosenthal, Y., Field P. and Sherrell, R., 1999, Precise determination of element/calcium ratios in calcareous samples using sector field inductively coupled plasma mass spectrometry: Analytical Chemistry, v. 71, p. 3248-3253

Schouten, S., Hopmans, E.C., Schefuss, E. and SinniNghe Damsté, J.S., 2002. Distributional variations in marine crenarchaeotal Membrane lipids: a new tool for reconstructing ancient sea water temperatures? Earth & Planetary Science Letters, v. 204, p. 265-274.

Schouten, S., Forster, A., Panoto, E.F. and Sinninghe Damste, J.S., 2007, Towards calibration of the TEX86 palaeothermometer for tropical sea surface temperatures in ancient greenhouse worlds: Organic Geochemistry, v. 38, p. 1537-1546.

Sluijs, A. and Brinkhuis, H., 2009, A dynamic climate and ecosystem state during the Paleocene-Eocene Thermal Maximum: inferences from dinoflagellate cyst assemblages on the New Jersey Shelf: Biogeosciences, v. 6, p. 1755-1781.

Sluijs, A., Brinkhuis, H., Crouch, E.M., John, C., Handley, L., Munsterman, D., Bohaty, S.M., Zachos, J.C., Reichart, G.-J., Schouten, S., Pancost, R.D., Damsté, J.S.S., Welters, N.L.D., Lotter, A.F. and Dickens, G.R., 2008, Eustatic variations during the Paleocene-Eocene greenhouse world: Paleoceanography, v. 23, PA4216, doi:10.1029/2008PA001615

Wade, B.S. and Pearson, P.N., 2008, Planktonic foraminiferal turnover, diversity fluctuations and geochemical signals across the Eocene/Oligocene boundary in Tanzania: Marine Micropaleontology, v. 68, p. 244-255.

Wade, B.S., Dutton, A., Rosenthal, Y., Olsson, R.K., Berggren, W.A. and Wright, J.D., 2009, Geochemistry of "glassy" planktonic foraminifera from the uppermost Eocene: implications of vital effects for reconstructing sea surface temperatures. In: Crouch, E.M., Strong, C.P., Hollis, C.J., (Eds.) Climatic and Biotic Events of the Paleogene (CBEP 2009): GNS Science Miscellaneous Series, v. 18, p. 155-156.

Wade, B.S., Pearson, P.N., Berggren, W.A. and Pälike, H., 2011, Review and revision of Cenozoic tropical planktonic foraminiferal biostratigraphy and calibration to the geomagnetic polarity and astronomical time scale: Earth Science Reviews, v. 104, p. 111-142.

Waters, L.A. and Mancini, E.A. 1982, Lithostratigraphy and biostratigraphy of upper Eocene and lower Oligocene strata in southwest Alabama and southwest Mississippi: Transactions – Gulf Coast Association of Geological Societies, v. XXXII, p. 303- 307.

Weijers, J.W.H., Schouten, S., Spaargaren, O.C. and Sinninghe Damsté, J.S., 2006, Occurrence and distribution of tetraether membrane lipids in soils: Implications for the use of the TEX86 proxy and the BIT index: Organic Geochemistry, v.37, p.1680-1693.

Zachos, J.C., Quinn, T.M. and Salamy, K.A., 1996, High-resolution ($10^4$ years) deep-sea foraminiferal stable isotope records of the Eocene-Oligocene climate transition: Paleoceanography, v.11, p.251-266.

Table DR1. Tie points used in the revised age model (in bold). MNT= Moody Branch Formation and N. Twistwood Creek Clay, CP= Cocoa Sand and Pachuta Marl, PS= Pachuta Marl and Shubuta Marl, BRB= Bumpnose and Red Bluff Formation.

| Bio- / Magnetostratigraphic Event | Depth (m) | Depth (feet) | Age (Ma) |
|---|---|---|---|
| **Top C12r** | **15.55** | **51.02** | **31.70** |
| HO *Pseudohastigerina* spp. | 21.34 | 70.00 | 32.00 |
| Base NP23 | 29.56 | 96.98 | 32.30 |
| Base NP22 | 33.50 | 109.91 | 32.80 |
| **$\delta^{13}$C IV** | **39.33** | **129.04** | **32.82** |
| **Top C13n** | **40.55** | **133.04** | **33.06** |
| **$\delta^{13}$C III** | **45.45** | **149.11** | **33.20** |
| **Top Hiatus ($\delta^{13}$C II)** | **46.25** | **151.75** | **33.39** |
| **Base Hiatus** | **46.25** | **151.75** | **33.55** |
| Base C13n | 46.36 | 152.10 | 33.55 |
| **SB 3 (PS-BRB) youngest** | **46.97** | **154.10** | **33.59** |
| **SB 3 (PS-BRB) oldest** | **46.97** | **154.10** | **33.62** |
| **HCO *Pseudohastigerina micra*** | **47.37** | **155.41** | **33.70** |
| **HO *Turborotalia cerroazulensis* group** | **49.38** | **162.00** | **33.77** |
| HO *Hantkenina* spp. | 49.68 | 162.99 | 33.70 |
| HO *Discoaster saipanensis* | 50.38 | 165.29 | 34.20 |
| **SB 1 (CP-PS) youngest ($\delta^{13}$C I)** | **50.38** | **165.29** | **34.01** |
| **SB 1 (CP-PS) oldest** | **50.38** | **165.29** | **35.00** |
| HO *Reticulofenestra reticulata* | 50.38 | 165.29 | 35.00 |
| Top C16n.1n | 53.64 | 175.98 | 35.34 |
| **SB (MNT- CP) youngest** | **53.95** | **177.00** | **35.40** |
| **SB (MNT-CP) oldest** | **53.95** | **177.00** | **35.90** |
| FAD *Isthmolithus recurvus* | 54.25 | 177.99 | 36.00 |
| Base C16n.2n | 54.25 | 177.99 | 36.34 |
| Top C17n | 64.40 | 211.29 | 36.62 |

In **Bold:** Tie-points included in age model

Table DR2. Planktic foraminiferal Mg/Ca values and paleotemperature

| Corrected Depth (m) | Corrected Depth (feet) | Age (Ma, this study) | Species | Mg/Ca mmol/mol | SSTs | SSTs +0.7°C |
|---|---|---|---|---|---|---|
| 35.97 | 118.00 | 32.665 | *T.ampliapertura* | 5.88 | 32.9 | 33.6 |
| 37.31 | 122.40 | 32.728 | *T.ampliapertura* | 4.65 | 30.3 | 31.0 |
| 38.53 | 126.40 | 32.786 | *T.ampliapertura* | 4.99 | 31.1 | 31.8 |
| 40.31 | 132.25 | 33.012 | *T.ampliapertura* | 3.07 | 25.7 | 26.4 |
| 43.04 | 141.20 | 33.128 | *D. pseudovenezuelana* | 4.48 | 29.9 | 30.6 |
| 45.78 | 150.20 | 33.276 | *T.ampliapertura* | 4.11 | 28.9 | 29.6 |
| 46.25 | 151.75 | 33.550 | *T.ampliapertura* | 2.92 | 25.1 | 25.8 |
| 46.28 | 151.85 | 33.552 | *T.ampliapertura* | 3.23 | 26.3 | 27.0 |
| 46.33 | 152.00 | 33.554 | *T.ampliapertura* | 3.56 | 27.3 | 28.0 |
| 46.59 | 152.85 | 33.569 | *T.ampliapertura* | 3.72 | 27.8 | 28.5 |
| 46.68 | 153.15 | 33.574 | *T.ampliapertura* | 3.47 | 27.1 | 27.8 |
| 46.71 | 153.25 | 33.576 | *T.ampliapertura* | 3.86 | 28.2 | 28.9 |
| 46.71 | 153.25 | 33.576 | *D. pseudovenezuelana* | 3.36 | 26.7 | 27.4 |
| 47.53 | 155.95 | 33.705 | *T.ampliapertura* | 3.74 | 27.9 | 28.6 |
| 47.69 | 156.45 | 33.710 | *T.ampliapertura* | 3.92 | 28.4 | 29.1 |
| 47.70 | 156.50 | 33.711 | *T.ampliapertura* | 4.14 | 29.0 | 29.7 |
| 47.78 | 156.75 | 33.713 | *T.ampliapertura* | 4.10 | 28.9 | 29.6 |
| 47.93 | 157.25 | 33.718 | *T.ampliapertura* | 3.46 | 27.0 | 27.7 |
| 47.96 | 157.35 | 33.719 | *T.ampliapertura* | 3.64 | 27.6 | 28.3 |
| 48.08 | 157.75 | 33.723 | *T.ampliapertura* | 3.83 | 28.1 | 28.8 |
| 48.20 | 158.15 | 33.727 | *T.ampliapertura* | 4.04 | 28.7 | 29.4 |
| 48.27 | 158.35 | 33.729 | *T.ampliapertura* | 4.18 | 29.1 | 29.8 |
| 48.33 | 158.55 | 33.731 | *T.ampliapertura* | 3.44 | 27.0 | 27.7 |
| 48.48 | 159.05 | 33.736 | *T.ampliapertura* | 3.38 | 26.8 | 27.5 |
| 48.69 | 159.75 | 33.743 | *T.ampliapertura* | 3.70 | 27.8 | 28.5 |
| 48.78 | 160.05 | 33.746 | *T.ampliapertura* | 3.92 | 28.4 | 29.1 |
| 48.86 | 160.30 | 33.748 | *T.ampliapertura* | 4.29 | 29.4 | 30.1 |
| 48.91 | 160.45 | 33.750 | *T.ampliapertura* | 4.33 | 29.5 | 30.2 |
| 49.26 | 161.60 | 33.761 | *T.ampliapertura* | 4.37 | 29.6 | 30.3 |
| 49.36 | 161.95 | 33.765 | *T.ampliapertura* | 3.92 | 28.4 | 29.1 |
| 49.45 | 162.25 | 33.783 | *T.ampliapertura* | 4.34 | 29.5 | 30.2 |
| 49.53 | 162.50 | 33.801 | *T.ampliapertura* | 4.19 | 29.2 | 29.9 |
| 49.67 | 162.95 | 33.834 | *T.ampliapertura* | 4.14 | 29.0 | 29.7 |
| 50.03 | 164.15 | 33.922 | *T.ampliapertura* | 4.43 | 29.8 | 30.5 |
| 50.19 | 164.65 | 33.958 | *T.ampliapertura* | 4.84 | 30.7 | 31.4 |
| 50.29 | 165.00 | 33.984 | *T.ampliapertura* | 5.54 | 32.3 | 33.0 |
| 50.38 | 165.29 | 34.005 | *T.ampliapertura* | 5.29 | 31.7 | 32.4 |

Table DR3. Planktic foraminiferal oxygen isotope results. Boxes indicate replicate analyses.

| Corrected Depth (m) | Corrected Mean Depth (ft) | Age (Ma, this study) | *P. naguewich-iensis* $\delta^{18}O$ | *T. ampliapertura* $\delta^{18}O$ | *H. alabamensis* $\delta^{18}O$ | *T.cerroazuelensis* $\delta^{18}O$ |
|---|---|---|---|---|---|---|
| 35.97 | 118.00 | 32.662 | -1.15 | - | - | - |
| 37.31 | 122.40 | 32.725 | -1.14 | -1.03 | - | - |
| 38.53 | 126.40 | 32.782 | -1.10 | -1.10 | - | - |
| 39.33 | 129.00 | 32.819 | -1.44 | - | - | - |
| 40.31 | 132.25 | 33.013 | -1.42 | -1.63 | - | - |
| 40.46 | 132.75 | 33.043 | - | - | - | - |
| 40.64 | 133.35 | 33.063 | - | - | - | - |
| 40.80 | 133.85 | 33.067 | -1.32 | - | - | - |
| 41.24 | 135.30 | 33.080 | - | - | - | - |
| 42.49 | 139.40 | 33.115 | - | - | - | - |
| 42.49 | 139.40 | 33.12 | -1.35 | - | - | - |
| 43.04 | 141.20 | 33.131 | -1.44 | -0.82 | - | - |
| 43.04 | 141.20 | 33.131 | - | - | - | - |
| 43.49 | 142.68 | 33.144 | -1.40 | -1.69 | - | - |
| 44.21 | 145.05 | 33.165 | -1.26 | -0.89 | - | - |
| 44.99 | 147.60 | 33.187 | -1.37 | - | - | - |
| 45.45 | 149.10 | 33.200 | - | - | - | - |
| 45.78 | 150.20 | 33.278 | -1.58 | -0.92 | - | - |
| 46.13 | 151.35 | 33.361 | -1.18 | - | - | - |
| 46.25 | 151.75 | 33.550 | - | -0.89 | - | - |
| 46.28 | 151.85 | 33.552 | -1.68 | -0.72 | - | - |
| 46.33 | 152.00 | 33.554 | -1.50 | -1.15 | - | - |
| 46.59 | 152.85 | 33.569 | -1.42 | -1.19 | - | - |
| 46.68 | 153.15 | 33.574 | -1.80 | -1.60 | - | - |
| 46.71 | 153.25 | 33.576 | -1.66 | -0.78 | - | - |
| 46.79 | 153.50 | 33.580 | -1.43 | -0.95 | - | - |
| 47.06 | 154.40 | 33.638 | - | - | - | - |
| 47.12 | 154.60 | 33.651 | -1.61 | - | - | - |
| 47.26 | 155.05 | 33.678 | -1.66 | - | - | - |
| 47.37 | 155.40 | 33.699 | -1.58 | - | - | - |
| 47.44 | 155.65 | 33.703 | -1.68 | -1.55 | - | - |
| 47.53 | 155.95 | 33.706 | -1.70 | -1.87 | - | - |
| 47.69 | 156.45 | 33.711 | -1.87 | -1.38 | - | - |
| 47.70 | 156.50 | 33.712 | -1.76 | -1.22 | - | - |
| 47.78 | 156.75 | 33.714 | -1.63 | -1.18 | - | - |
| 47.78 | 156.75 | 33.714 | -1.47 | -1.57 | - | - |
| 47.93 | 157.25 | 33.720 | -2.04 | -1.80 | - | - |
| 47.96 | 157.35 | 33.721 | -1.36 | -1.87 | - | - |
| 48.08 | 157.75 | 33.725 | -1.64 | -1.06 | - | - |
| 48.20 | 158.15 | 33.729 | -1.68 | -1.45 | - | - |
| 48.27 | 158.35 | 33.731 | -1.85 | -1.45 | - | - |
| 48.27 | 158.35 | 33.731 | - | -1.53 | - | - |
| 48.33 | 158.55 | 33.733 | -1.92 | -1.43 | - | - |
| 48.48 | 159.05 | 33.739 | -1.38 | -1.42 | - | - |
| 48.69 | 159.75 | 33.746 | -1.50 | -1.65 | - | - |
| 48.78 | 160.05 | 33.749 | -1.85 | -1.92 | - | - |
| 48.86 | 160.30 | 33.752 | -1.78 | -1.59 | - | - |
| 48.91 | 160.45 | 33.754 | -1.77 | -2.04 | - | - |
| 49.05 | 160.93 | 33.759 | - | - | - | - |

Table DR3. Planktic foraminiferal oxygen isotope results. Boxes indicate replicate analyses.

| | | | | | | |
|---|---|---|---|---|---|---|
| 49.06 | 160.95 | 33.759 | -1.73 | - | - | - |
| 49.26 | 161.60 | 33.766 | -1.75 | -1.81 | - | - |
| 49.36 | 161.95 | 33.769 | -1.91 | -1.73 | -2.02 | - |
| 49.45 | 162.25 | 33.788 | -1.83 | -1.86 | -1.95 | - |
| 49.45 | 162.25 | 33.788 | -1.88 | - | - | - |
| 49.45 | 162.25 | 33.788 | -1.86 | - | - | - |
| 49.53 | 162.50 | 33.806 | -1.84 | -1.77 | -2.19 | - |
| 49.67 | 162.95 | 33.839 | -1.96 | -1.78 | -2.06 | -1.49 |
| 49.67 | 162.95 | 33.839 | - | -1.81 | - | - |
| 49.74 | 163.20 | 33.858 | -1.50 | - | -1.06 | - |
| 49.94 | 163.85 | 33.905 | -1.86 | -1.55 | -2.32 | - |
| 50.03 | 164.15 | 33.927 | -1.80 | -1.76 | -1.81 | - |
| 50.19 | 164.65 | 33.963 | -1.87 | -1.90 | -2.18 | - |
| 50.29 | 165.00 | 33.989 | -1.76 | -2.02 | -1.48 | - |
| 50.34 | 165.15 | 34.000 | -2.24 | -2.27 | -1.79 | - |
| 50.34 | 165.15 | 34.000 | - | -2.04 | - | - |

Table DR4. Organic geochemistry results and paleotemperatures. Samples with a branched isoprenoid tetraether (BIT) index with values >0.4 were discarded, since this may point towards elevated input of GDGTs from soil organic matter and may have obscured TEX86 paleothermometry (Weijers et al., 2006).

| Sample | Depth (feet) | Depth (m) | Age (Ma, this study) | SST (°C $TEX_{86}^{L}$) | SST (°C $TEX_{86}^{H}$) | BIT- index | |
|---|---|---|---|---|---|---|---|
| SSQ05 | 76.05 | 23.18 | 32.061 | 23.6 | 28.7 | 0.10 | |
| SSQ06 | 80.65 | 24.58 | 32.127 | 23.9 | 28.4 | 0.07 | |
| SSQ07 | 85.25 | 25.98 | 32.194 | 21.8 | 27.7 | 0.10 | |
| SSQ08 | 90.05 | 27.45 | 32.263 | 21.3 | 27.9 | 0.08 | |
| SSQ09 | 95.45 | 29.09 | 32.341 | 21.1 | 28.3 | 0.07 | |
| SSQ10 | 100.25 | 30.56 | 32.410 | 20.8 | 27.9 | 0.07 | |
| SSQ11 | 104.95 | 31.99 | 32.477 | 21.6 | 28.3 | 0.08 | |
| SSQ12 | 110.05 | 33.54 | 32.551 | 21.4 | 28.2 | 0.07 | |
| SSQ13 | 115.05 | 35.07 | 32.623 | 21.2 | 27.9 | 0.09 | |
| SSQ14 | 120.30 | 36.67 | 32.699 | 22.5 | 28.9 | 0.09 | |
| Pilot 1 | 126.35 | 38.51 | 32.786 | 22.8 | 28.9 | 0.09 | |
| SSQ15 | 130.60 | 39.81 | 32.918 | 24.5 | 29.1 | 0.11 | |
| SSQ16 | 134.95 | 41.13 | 33.075 | 18.8 | 27.7 | 0.83 | |
| SSQ34 | 136.15 | 41.50 | 33.085 | 17.7 | 27.7 | 0.77 | |
| Pilot 2 | 138.05 | 42.08 | 33.101 | 19.0 | 27.7 | 0.77 | |
| SSQ17 | 139.65 | 42.57 | 33.115 | 19.2 | 28.2 | 0.66 | |
| SSQ35 | 141.75 | 43.21 | 33.132 | 20.3 | 28.4 | 0.16 | |
| SSQ36 | 143.05 | 43.60 | 33.144 | 20.1 | 29.0 | 0.15 | |
| SSQ18 | 144.65 | 44.09 | 33.157 | 20.6 | 28.2 | 0.28 | |
| SSQ37 | 146.40 | 44.62 | 33.172 | 20.9 | 28.8 | 0.14 | |
| SSQ38 | 148.45 | 45.25 | 33.189 | 20.8 | 28.7 | 0.22 | |
| SSQ39 | 149.25 | 45.49 | 33.206 | 21.3 | 28.4 | 0.18 | |
| Pilot 3 | 151.25 | 46.10 | 33.350 | 20.7 | 28.1 | 0.21 | |
| SSQ40 | 152.15 | 46.38 | 33.556 | 20.3 | 28.8 | 0.34 | |
| SSQ19 | 152.93 | 46.61 | 33.570 | 20.1 | 28.0 | 0.31 | |
| SSQ41 | 153.35 | 46.74 | 33.577 | 20.8 | 28.1 | 0.29 | |
| SSQ42 | 154.80 | 47.18 | 33.663 | 21.2 | 28.3 | 0.17 | |
| SSQ43 | 156.15 | 47.59 | 33.707 | 23.2 | 28.8 | 0.16 | |
| Pilot 4 | 156.95 | 47.84 | 33.715 | 21.6 | 28.5 | 0.15 | |
| SSQ44 | 158.00 | 48.16 | 33.726 | 21.8 | 28.7 | 0.10 | |
| SSQ45 | 159.35 | 48.57 | 33.739 | 22.3 | 29.1 | 0.08 | |
| SSQ20 | 161.18 | 49.13 | 33.757 | 24.2 | 30.0 | 0.08 | |
| SSQ46 | 162.05 | 49.39 | 33.769 | 23.9 | 30.1 | 0.06 | |
| Pilot 5 | 163.05 | 49.70 | 33.841 | 23.4 | 30.0 | 0.06 | |
| SSQ47 | 163.75 | 49.91 | 33.892 | 24.5 | 30.7 | 0.05 | |
| SSQ48 | 164.55 | 50.15 | 33.950 | 23.9 | 30.6 | 0.04 | |
| SSQ49 | 165.65 | 50.49 | 35.012 | 22.7 | 29.3 | 0.06 | |
| SSQ21 | 166.55 | 50.76 | 35.043 | 21.8 | 28.9 | 0.08 | |
| SSQ50 | 167.65 | 51.10 | 35.080 | 22.8 | 29.4 | 0.07 | |
| SSQ51 | 168.45 | 51.34 | 35.108 | 22.5 | 29.1 | 0.08 | |
| SSQ22 | 169.65 | 51.71 | 35.149 | 23.1 | 29.7 | 0.06 | |